Journal of Mines, Metals and Fuels, *73(5): 1247-1256; 2025. DOI: 10.18311/jmmf/2025/48627*

Print ISSN : 0022-2755

Journal of Mines, Metals and Fuels

Contents available at: *www.informaticsjournals.co.in/index.php/jmmf*

Failure Investigation of the Driving Shaft in an Industrial Paddle Mixer

Sukhadip Mhankali Chougule[1,2], Govindarajan Murali[1*] and Anant Sidhappa Kurhade[3,4]

[1]Department of Mechanical Engineering, Koneru Lakshmaiah Education Foundation, Green Fields, Vaddeswaram, Guntur (Dt) - 522502, Andhra Pradesh, India; muralinitt@gmail.com

[2]Department of Mechanical Engineering, PCET's Pimpri Chinchwad College of Engineering and Research, Ravet, Pune - 412101, Maharashtra, India

[3]Department of Mechanical Engineering, Dr. D. Y. Patil Institute of Technology, Sant Tukaram Nagar, Pimpri, Pune - 411018, Maharashtra, India

[4]School of Technology and Research, Dr. D. Y. Patil Dnyan Prasad University, Sant Tukaram Nagar, Pimpri, Pune - 411018, Maharashtra, India

Abstract

This study focuses on the failure analysis and structural evaluation of the shaft in a double-shaft paddle mixer, a vital component in industrial mixing processes used in food processing, fertilizer production, and pharmaceutical manufacturing. The mixer is designed to blend materials of different densities, sizes, and viscosities efficiently through a centrally mounted horizontal shaft that rotates inside a cylindrical chamber. The system includes paddles for agitation, feed openings for material input, and a discharge valve for controlled output. A primary concern in this research is the mechanical failure of the driving shaft, which transmits power from the motor via a gear drive. Structural weaknesses and failure mechanisms were investigated by analysing system pressure, bending moments, and externally applied forces. Stress distributions were computed to identify critical failure locations that could compromise the shaft's integrity. A three-dimensional (3D) model of the shaft was developed using Pro-E software to enhance accuracy. Finite Element Analysis (FEA) was performed using ANSYS 13.0 to determine stress distribution, deformation, and failure-prone regions under operational loads. The numerical results were cross-verified with theoretical calculations based on ASME design codes to validate the structural adequacy. A shaft prototype was fabricated and tested under actual operating conditions to confirm the computational findings further. Experimental results closely matched FEA predictions, proving the effectiveness of the proposed design modifications. The optimised shaft exhibited increased durability, improved structural integrity, and enhanced performance. This research underscores the importance of virtual simulations before manufacturing, demonstrating how predictive analysis minimises failure risks. The study contributes to cost-efficient, time-saving design improvements, reducing material waste while ensuring the reliability of industrial mixing systems. These findings have broad implications for improving durability and efficiency in mechanical systems.

Major Findings: *The study identifies excessive bending moments, torsional stress, material fatigue, and improper loading conditions as primary causes of shaft failure. A FEA using ANSYS 13.0 was conducted, and results were validated through experimental testing, confirming the reliability of design modifications. The optimised shaft design enhances durability, structural integrity, and operational efficiency, reducing failure risks and improving industrial mixing performance.*

Keywords: *Bending Moment, Failure Analysis, Finite Element Analysis (FEA), Gear Drive, Shaft Design, Structural Evaluation*

**Author for correspondence*

1.0 Introduction

The driving shaft is a critical component in industrial mixing equipment, transmitting rotational power from the motor to the mixing paddles. In double-shaft paddle mixers, the shaft undergoes continuous mechanical loading, torque, bending forces, and fatigue stresses, making it susceptible to structural failure over time. A failure in the shaft can lead to unplanned downtime, increased maintenance costs, and reduced operational efficiency in industries such as food processing, pharmaceuticals, and fertilizer production. The failure investigation of the driving shaft in an industrial paddle mixer involves a comprehensive analysis of potential causes, including material defects, improper repair techniques and operational stresses. The driving shaft is a critical component, and its failure can lead to significant operational disruptions. The investigation typically involves examining the shaft's material properties, design, and repair history to identify the root cause of failure. Shafts are among the most frequently weld-repaired industrial components, but improper welding can significantly contribute to their failure, even when performed with high quality. This study examines the failure analysis of weld-repaired steel shafts, highlighting common failure modes, repair methods, and case studies from various industries[1]. A comprehensive approach was employed to identify the root cause(s) of premature failure in a pelletizer mixer timing gear, encompassing field examination, interviews, lubrication analysis, metallurgical testing, and fracture surface evaluation. The findings revealed surface hardness deficiencies, with pitting and crack propagation linked to high contact stresses and inadequate surface strength, ultimately leading to failure[2]. The study examines the failure of an industrial cooling water pump's drive shaft, revealing that the shaft and key failed due to material processing issues. Detailed analysis, including hardness testing and fractography, identified hardness variation in the shaft as the root cause, leading to plastic deformation, key rattling, fatigue cracking, and eventual shaft failure by torsional shear[3]. The study analyses the failure of a shaft connected to blades, determining the root cause through visual inspection, microscopy, and hardness testing. The failure was attributed to fatigue caused by improper welding and recommended remedies were provided to prevent or delay future occurrences[4]. Fatigue design of materials in rotary equipment is crucial, especially as fatigue failures in the petroleum sector have risen. This study analyses crankshaft failure, revealing brittle fracture with crack initiation at sharp graphite boundaries in a pearlitic matrix, leading to fracture propagation and failure[5]. Pumps play a crucial role in the petroleum industry, but component failures necessitate failure analysis to identify the cause and mode of failure. This study utilises a Scanning Electron Microscope (SEM) for fracture pattern observation and material verification of the pump shaft[6]. This paper investigates the failure of a non-drive shaft in a conveyor at a coke plant, aiming to identify the root cause and contributing factors. Methods such as visual examination, microscopy, chemical analysis, mechanical testing, and life calculations revealed that the fracture surface of the 45C8 grade shaft indicated rotating bending fatigue failure[7]. This study uses the Discrete Element Method (DEM) with the Plackett–Burman experimental design to investigate the factors influencing the mixing performance of double-shaft, batch-type paddle mixers. The analysis of material properties, operational conditions, and geometric parameters shows that geometric factors significantly affect energy consumption without influencing mixing quality or time, highlighting their potential for designing more efficient and sustainable mixers[8]. The automotive industry invests heavily in Research and Development, yet component failures persist due to defects. This study presents a failure analysis of a police car's drive bar, revealing that pre-existing defects and an unfavourable microstructure led to brittle fracture and premature failure, as shown through light optical and SEM[9]. The main drive in a raw mill is critical for operation, and failures can disrupt the entire process. This study uses vibration analysis for predictive maintenance, identifying misalignment in the LS symetro gear as the root cause of vibration, with a proposed solution of heat treatment to reduce shaft misalignment[10]. The paper analyses the failure of an intermediate shaft in a prototype, identifying bending caused by fatigue due to improper design. The study highlights the importance of considering stress factors and design details to prevent fatigue and ensure long service life[11]. The overview provides insights into the dominant fracture mechanisms in mechanical metallic components under industrial service conditions, emphasising their relationship with operating parameters and loading conditions. It also summarises failure investigation and prevention approaches, offering a holistic view of frameworks for risk minimisation and quality improvement[12]. Researchers examine fatigue fracture in industrial components, using case histories of track-type

chain blocks and steel rebars to correlate failure modes with operating conditions. It also presents failure prevention methodologies, emphasizing a process and systems approach to minimize risks and enhance quality and business performance[13]. Smartphones (2-6W) struggle with heat from demanding applications like gaming and cameras. This research explores using passive Phase Change Material (PCM) cooling to keep components below 85°C, a better option than standard methods like convection and heat pipes, which struggle with high power[14]. Simulations tested FR4, silicon, and copper-clad boards with nine components under various airflow conditions[15]. Copper cladding significantly lowered component temperatures (30-47°C at 5 m/s), reduced required airflow (by 2 m/s), and improved IC chip cooling (1.50-11.12°C) compared to the other materials. A novel minichannel PCM system for cooling different IC chips was also analysed, showing N-Eicosane's superiority (reducing temperature from 53.234°C to 51.520°C, a further 0.5°C and 1.35°C improvement over paraffin wax and ATP 78, respectively)[16]. Further research covers mini jet impingement cooling[17], nanofluids[18], water-saving faucets[19], and twisted tape heat transfer enhancement[20-22]. A review of electronic cooling technologies explores challenges and advancements in harsh environments, while a study on *Calophyllum inophyllum* biodiesel with dimethyl carbonate focuses on optimising engine performance and emissions. Research on solar collectors using recycled aluminium cans enhances drying efficiency, and numerical analysis investigates substrate board thermal conductivity for electronic cooling. Additionally, aerodynamic efficiency is optimised through CFD and wind tunnel experiments, and fuzzy logic techniques are applied to predict heat transfer enhancement with twisted tape inserts in heat exchangers[23-31]. Studies on wavy corrugated twisted tape inserts in double-pipe heat exchangers demonstrate significant heat transfer enhancement, with performance analysis highlighting their effectiveness in forced convection. Research on electronic cooling explores thermal performance across different substrate materials and advanced solutions for harsh environments, including PCM integration for smartphone circuit cooling. Additionally, wind rose analysis assesses temperature variation in wind turbines using sensor implantation. At the same time, numerical and experimental investigations examine the influence of overlapping angles on the strength and deformation of arc-welded curved plates[32-40]. A comparative study of mono-composite and metal leaf springs evaluates experimental and numerical performance, while real-time surface finish measurement of stepped holding shafts is automated for precision. CFD simulations analyse heat transfer in counter-flow helical double-pipe heat exchangers, and an algorithmic approach automates HVACR duct design. Nanofluid applications enhance heat transfer in double-pipe heat exchangers, while an integrated vehicle safety approach explores novel bumper designs with energy-absorbing mechanisms. Additionally, green adsorbents are investigated for heavy metal removal, focusing on zinc ion uptake by *Tinospora cordifolia* biocarbon[41-47]. An investigation into the effect of transformation-induced plasticity steel plate thickness on the ultimate tensile strength of Nd: YAG laser butt-welded joints reveals its impact on weld integrity, while an experimental study examines the mechanical behaviour of mild steel curved plates under varying thicknesses. Computational research explores the thermal management of IC chips using phase change materials, and fuzzy logic modelling predicts heat transfer performance in double-pipe heat exchangers with wavy twisted tape inserts. Additionally, the influence of oxygen-containing additives in unleaded gasoline on exhaust emissions is analysed for potential environmental benefits[48-51].

This research examines the failure mechanisms of the driving shaft in an industrial paddle mixer, aiming to determine the root causes, assess stress distribution, and enhance the shaft's design for more excellent durability. Key factors contributing to failure include high bending moments, torsional stress, material fatigue, and improper loading conditions. A comprehensive failure analysis, integrating FEA and experimental validation, is crucial for identifying vulnerabilities and implementing practical solutions.

2.0 Paddle Mixer Design

1.1 Twin-Shaft Paddle Mixer

Double-shaft paddle mixers are widely used in the food, fertilizer, and pharmaceutical industries to blend various materials, including solids and liquids as shown in Figure 1 and Figure 2. These mixers utilise counter-rotating paddles to ensure uniform mixing, with key components such as a motor-driven shaft, paddles, and a gear drive. They provide advantages like uniform mixing, minimal heat generation, low energy consumption, reduced material segregation, and easy maintenance. Suitable for

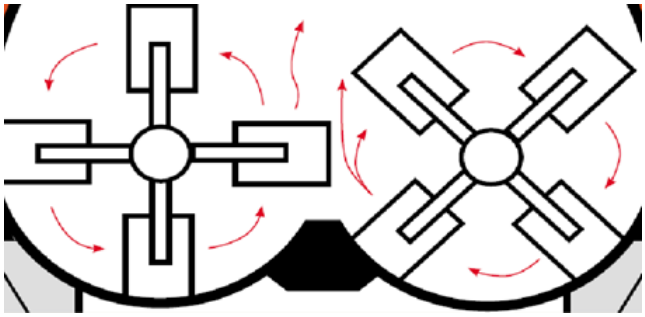


Figure 1. Double shaft paddle mixer.

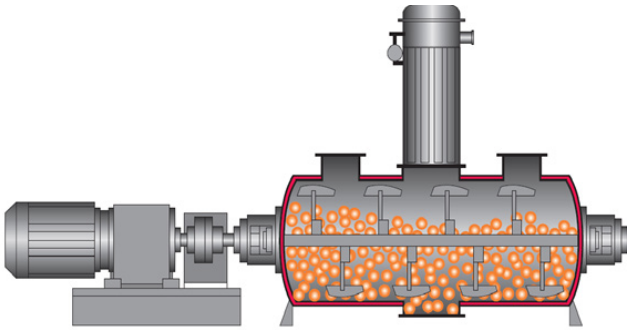


Figure 2. Mixer working.

processing powders, granules, fibres, moist solids, and viscous substances, these mixers create a fluidized zone for thorough blending and a transport zone for material movement. Ingredients are continuously fed, allowing the injection of liquids, while shear mixing occurs between the paddles and the chamber walls.

3.0 Paddle Shaft Calculation Parameters

The parameters used in paddle shaft calculations are explained in Table 1.

3.1 Calculating Unknown Parameters

Knowing the bar and paddle masses allows the calculation of the shaft's reaction force, stress, and required diameter.

Bar mass = 0.8659 kg
Paddle mass = 1.2607 kg
Total mass (1 unit) = 2.591 kg
Total weight (1 unit) = 25.4177 N

Table 1. Parameters table

Sr. No	Parameter Description	Notations	Values
1	Mass of Bar	M bar	0.8659 kg.
2	Mass of Paddle	M paddle	1.2607 kg
3	Reaction at point A	Ra	Not specified
4	Reaction at point B	Rb	Not specified
5	Ultimate Tensile Strength	Sut	460 N/mm²
6	Yield Strength	Syt	250 N/mm²
7	Factor of Safety	FOS	2
8	Required Speed (rpm)	N	38 rpm
9	Shock Factor	Kb	1.5
10	Fatigue Factor	Kt	1
11	Power of Motor	P	11 KW
12	Pressure on Paddle Shaft	Pi	$7.7 * 10^{-2}$ N/mm²
13	Outer Diameter of the Pipe	do	Not specified

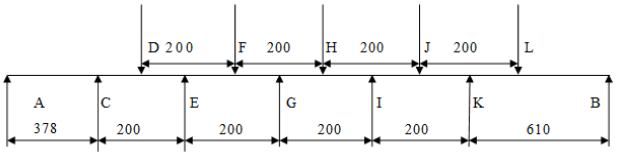


Figure 3. Diagram of vertical loads for determining bending moments.

3.1.1 Vertical Loading Diagram

A vertical loading diagram is considered with ten-point loads (both upward and downward) on a fixed-end pipe (A and B) as explained in Figure 3. Reactions at the fixed supports, including bending moments, are calculated.

3.1.1.1 Reactions

$$+$$

$$\sum MA = 0$$

$$(-Rb \times 2788) + (25.771 \times 2178) - (25.771 \times 1978) + (25.771 \times 1778) - (25.771 \times 1578) + (25.771 \times 1378) - (25.771 \times 1178) + (25.771 \times 978) - (25.771 \times 778) + (25.771 \times 578) - (25.771 \times 378) = 0$$

$$(-RB \times 2788) + 25261.94 = 0$$

Rb* = 9.06 *N
Ra + *Rb* = 0
Ra* = –9.06 *N

3.1.1.2 Bending Moment Calculations

BmA = 0, *BmB* = 0
BmC = (–9.06 × 578) + (25.771 × 200)
= –153.08 *N.mm*
BmE = (–9.06 × 778) + (25.771 × 400) – (25.771 × 200)
= –1965.08 *N.mm*
BmF = (–9.06 × 978) + (25.771 × 600) – (25.771 × 400) + (25.771 × 200)
= –1306.52 *N.mm*
BmG = (–9.06 × 1178) + (25.771 × 800) – (25.771 × 600) + (25.771 × 400) – (25.771 × 200)
= –505.48 *N.mm*
BmH = (–9.06 × 1378) + (25.771 × 1000) – (25.771 × 800) + (25.771 × 600) – (25.771 × 400) + (25.771 × 200)
= 2766.12 *N.mm*
BmI = (–9.06 × 1578) + (25.771 × 1200) – (25.771 × 1000) + (25.771 × 800) – (25.771 × 600) + (25.771 × 400) – (25.771 × 200)
= 954.12 *N.mm*
BmJ = (–9.06 × 1778) + (25.771 × 1400) – (25.771 × 1200) + (25.771 × 1000) – (25.771 × 800) + (25.771 × 600) – (25.771 × 400) + (25.771 × 200)
= 4225.72 *N.mm*
BmK = (–9.06 × 1978) + (25.771 × 1600) – (25.771 × 1400) + (25.771 × 1200) – (25.771 × 1000) + (25.771 × 800) – (25.771 × 600) + (25.771 × 400) – (25.771 × 200)
= 2413.72 *N.mm*
BmL = (–9.06 × 2178) + (25.771 × 1800) – (25.771 × 1600) + (25.771 × 1400) – (25.771 × 1200) + (25.771 × 1000) – (25.771 × 800) + (25.771 × 600) – (25.771 × 400) + (25.771 × 200)
= 5685.32 *N.mm*

3.1.2 Horizontal Loading Diagram

Figure 4 illustrates nine loads applied to the pipe. Based on the loading conditions, the bending moment reactions are calculated at the fixed ends A and B.

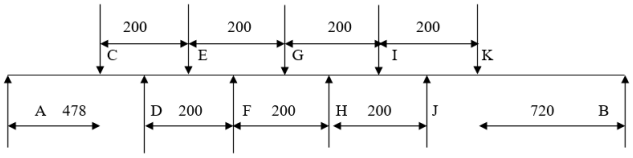


Figure 4. A horizontal loading diagram is used to calculate bending moments.

3.1.2.1 Reactions

∑mA = 0
(–*Rb* × 2788) + (23.76 × 478) – (23.76 × 678) + (23.76 × 878) – (23.76 × 1078) + (23.76 × 1278) – (23.76 × 1478) + (23.76 × 1678) – (23.76 × 1878) + (23.76 × 2078) = 0
(–*Rb* × 2788) + (30398.84) = 0
Rb* = 10.90 *N
Ra + *Rb* – 23.76 = 0
Ra + 10.90 – 23.76 = 0
Ra* = 12.86 *N

3.1.2.2 Bending Moment Calculations

BmA = 0, *BmB* = 0
BmC = (12.86 × 478)
= (6147.08) *N.mm*
BmD = (12.86 × 678 – (23.76 × 200)
= 3967.38 *N.mm*
BmE = (12.86 × 878) – (23.76 × 400) + (23.76 × 200)
= 6539.08 *N.mm*
BmF = (12.86 × 1078) – (23.76 × 600) + (23.76 × 400) – (23.76 × 200)
= 2359.08 *N.mm*
BmG = (12.86 × 1278) – (23.76 × 800) + (23.76 × 600) – (23.76 × 400) + (23.76 × 200)
= 6828.84 *N.mm*
BmH = (12.86 × 1478) – (23.76 × 1000) + (23.76 × 800) – (23.76 × 600) + (23.76 × 400) – (23.76 × 200)
= 4751.08 *N.mm*
BmI = (12.86 × 1678) – (23.76 × 1200) + (23.76 × 1000) – (23.76 × 800) + (23.76 × 600) – (23.76 × 400) + (23.76 × 200)
= 7323.08 *N.mm*
BmJ = (12.86 × 1878) – (23.76 × 1400) + (23.76 × 1200) – (23.76 × 1000) + (23.76 × 800) – (23.76 × 600) + (23.76 × 400) – (23.76 × 200)
= 5143.08 *N.mm*

BmJ = (12.86 × 2078) – (23.76 × 1600) + (23.76 × 1400) – (23.76 × 1200) + (23.76 × 1000) – (23.76 × 800) + (23.76 × 600) – (23.76 × 400) + (23.76 × 200)

= 771508 *N.mm*

Max Bending moment from VLD and HLD by triangle law

$$\frac{X}{710}=\frac{Y}{610}$$

$$\frac{7715.08}{710}=\frac{Y}{610}$$

$Y = Mb$ = 6628.449 *N.mm*

By properties of Structural Steel,

$$Sut = 460\,{}^{N}\!/_{mm^2}$$

$$Syt = 250\,{}^{N}\!/_{mm^2}$$

According to the ASME code Permissible shear stress τ max is,

τmax = 0.30 *Syt*

Or

τmax = 0.18 *Sut*

Whichever is the minimum is selected.

$$0.30\ Syt = 0.30(250) = 75\,{}^{N}\!/_{mm^2}$$

$$0.18\ Sut = 0.18(460) = 82.8\,{}^{N}\!/_{mm^2}$$

From above, we choose τ max $= 82.8\,{}^{N}\!/_{mm^2}$

Consider the Factor Of safety = 2

$$\tau per = \frac{\tau}{FOS}$$

$$\frac{82.8}{2} = 41.4\,{}^{N}\!/_{mm^2}$$

Torque Obtained

$$P = \frac{2\pi NMt}{60}$$

$$Mt = \frac{60\times10^{6}\times11}{2\pi\times38}$$

Mt = 2764270.06 *N.mm*

Mb = 6628.449 *N.mm*

3.1.3 Design of Shaft Based on ASME Code

As the Shaft bears gradual loading conditions, values of shock and fatigue factors Kb and Kt are,

Kb = 1.5, Kt = 1.0

$$c = \frac{di}{do}$$

Take c = 0.888

$$\tau = \frac{16}{\pi do^3\left(1-c^4\right)}\sqrt{\left(Mb^2+Mt^2\right)}$$

$$\tau = \frac{16}{\pi do^3\left(1-0.888^4\right)}\times\sqrt{\left(6628.44^2+2764270.06^2\right)}$$

do = 87.69 *mm*

do* = 90 *mm

As c = 0.888

$$c = \frac{di}{do}$$

0.888 * 90 = *di*

di* = 80 *mm

3.1.4 Pressure Applied on the Shaft Given as Per the Process Requirement,

$$\boldsymbol{Pi = 7.7\times10^{-2}\,{}^{N}\!/_{mm^2}}$$

3.3.5 Force applied on shaft

$F = P \times A(surface\ area)$

$= P \times 2\pi(R - r) \times l$

$= 7.7 \times 10^{-2} \times 2\pi(45 - 40) \times 2044$

F* = 4944.489 *N

3.1.5 Stress on the Shaft

$$\sigma = \frac{F}{c/s\ area}$$

$$\sigma = \frac{4944.489}{\pi/4\left(90-80\right)^2}$$

$$\boldsymbol{\sigma = 62.95\,{}^{N}\!/_{mm^2}}$$

The allowable stress is the value used in design to determine the component's dimensions, representing the stress that should not be exceeded under normal operating conditions. For ductile materials, the allowable stress σ is calculated using the formula:

$$\sigma max = Syt/FOS$$

For structural steel, Syt is 250 MPa, so:

$$\sigma max = 250/2 = 125 \text{ MPa}$$

This value gives the stress on the pipe

4.0 Results

This study successfully analysed the failure mechanisms of the driving shaft in a double – shaft paddle mixer, focusing on stress distribution, bending moments, and torsional forces. The findings revealed that excessive bending and material fatigue were key contributors to failure. FEA and experimental validation confirmed the reliability of the optimised shaft design. The improved design enhances durability, structural integrity, and operational efficiency, reducing failure risks. This research highlights the importance of predictive analysis in ensuring reliable and cost – effective industrial mixing solutions. The quantitative results are shown in Table 2.

1. **Loading Analysis**: The analysis considers both vertical and horizontal loading scenarios, with ten – point loads acting on the pipe in the vertical case and nine loads in the horizontal case. Reactions at fixed support A and B are calculated for both scenarios, providing the basis for determining bending moments along the shaft.
2. **Bending Moment Calculations**: Bending moments are calculated at various points along the shaft under vertical and horizontal loading conditions. The maximum bending moment is identified as Mb = 6628.449 *N.mm*, derived using the triangle law.
3. **Material Properties and Stress Analysis**: The shaft material is identified as structural steel, with given values for Ultimate Tensile Strength (Sut) and Yield Strength (Syt). Using the ASME code, the permissible shear stress (τmax) is calculated, and considering a safety factor, the allowable shear stress (τper) is determined.

Table 2. Quantitative results

Parameter	Value
Maximum Bending Moment (Mb)	6628.449 N·mm
Ultimate Tensile Strength (Sut)	460 N/mm²
Yield Strength (Syt)	250 N/mm²
Permissible Shear Stress (τ_max)	82.8 N/mm²
Factor of Safety (FOS)	2
Torque Acting on Shaft (Mt)	2,764,270.06 N·mm
Outer Shaft Diameter (do)	90 mm
Inner Shaft Diameter (di)	80 mm
Pressure Applied on Shaft (Po)	7.7×10^{-2} N/mm²
Force Acting on Shaft (F)	4944.489 N

4. **Torque and Shaft Design**: The torque acting on the shaft (Mt) is calculated based on the motor power and rotational speed. Using the combined bending and torsional moments, the shaft's outer diameter (do) is calculated to be 90 mm, and the inner diameter (di) is determined to be 80 mm.
5. **Pressure and Stress on Shaft**: Given the pressure applied to the shaft (Po), the force acting on the shaft is calculated, considering the surface area. The stress on the shaft due to this force is calculated, resulting in σ = 62.95 N/mm².

5.0 Conclusion

This study effectively examined the structural integrity of the driving shaft in a double – shaft paddle mixer, a critical component in industrial mixing applications. The analysis assessed the shaft's performance under operational loads, considering both vertical and horizontal loading conditions to develop a comprehensive understanding of the forces involved. The maximum bending moment (Mb = 6628.449M_b = 6628.449Mb = 6628.449 N·mm) was a key factor in guiding design improvements. Using the mechanical properties of structural steel, such as Ultimate Tensile Strength (SutS_{ut}Sut) and Yield Strength (SytS_{yt}Syt), along with ASME code guidelines, permissible and allowable shear stress values were determined to ensure compliance with safety standards. Additionally, the torque on the shaft (Mt = 2,764,270.06M_t = 2,764,270.06Mt = 2,764,270.06 N·mm), calculated based on motor power and rotational speed, played a crucial role in defining shaft dimensions.

The optimised design, with an outer diameter of 90mm and an inner diameter of 80mm, provides sufficient strength and rigidity to endure applied forces. The study also evaluated the impact of pressure (Po = 7.7 × 10−2P_o = 7.7 \times 10^{ – 2}Po = 7.7 × 10−2 N/mm²), leading to a force of 4944.489 N and a stress value of 62.95 N/mm². Since this stress remains within the allowable limit of 125 MPa for structural steel, the shaft was confirmed to operate safely under real – world conditions. Overall, the results validate the robustness of the shaft design, ensuring its durability and reliability in industrial operations. This research forms a strong foundation for manufacturing and performance testing. Future work may involve further refinements through advanced FEA and experimental validation to optimize the design and enhance efficiency.

6.0 References

1. Miller BA, Taylor RO, Swartzentruber PD, Kelly BP. Failure of steel shafts due to improper repair welding. J Fail Anal Prev. 2023; 23(2):894–909. https://doi.org/10.1007/s11668 – 023 – 01629 – 4
2. Merah N, Al – Qutub A. Premature failure of an industrial mixer timing gears. J Fail Anal Prev. 2017; 17:871–881. https://doi.org/10.1007/s11668 – 017 – 0300 – 9
3. Sondar PR, Kumar JR, Chawla S, Dsilva PC, Hegde SR. Failure of a cooling water pump shaft. J Fail Anal Prev. 2021; 21:149–159. https://doi.org/10.1007/s11668 – 020 – 01043 – 0
4. Pelaseyed SS, Mashayekhi F, Movahedi – Rad A. Investigation of the shaft failure connected to extruder. J Fail Anal Prev. 2015; 15:775–781. https://doi.org/10.1007/s11668 – 015 – 0030 – 9
5. Chidambaram S. Failure investigation of an industrial crankshaft made of ductile iron. Carbon. 2017; 3:3–90.
6. Nugroho R, Tri Iswanto P. Failure analysis of the broken oil industrial drive shaft pump components due to dynamics load. InAIP Conference Proceedings 2023; 2654(1). AIP Publishing. https://doi.org/10.1063/5.0128582
7. Palit P, Pal U, Gokarn P, Kanrar S. Revamping shaft design for combating fatigue failure. J Fail Anal Prev. 2021; 21:138–148. https://doi.org/10.1007/s11668 – 020 – 01039 – w
8. Emmerink J, Hadi A, Jovanova J, Cleven C, Schott DL. Parametric analysis of a double shaft, batch – type paddle mixer using the Discrete Element Method (DEM). Processes. 2023; 11(3):738. https://doi.org/10.3390/pr11030738
9. Barbosa C, Do Nascimento JL, Caminha IM, de Cerqueira Abud I, de Carvalho SS. A microstructural and fractographic study on the failure of a drive shaft. J Fail Anal Prev. 2011; 11:693–699. https://doi.org/10.1007/s11668 – 011 – 9499 – z
10. Alrasyid L, Malta J. Analisis kerusakan melalui predictive maintenance pada main drive raw mill indarung II/III. METAL: Jurnal Sistem Mekanik dan Termal. 2019; 3(2):68–72.
11. Mandal SK, Karmakar PM. Analysis of an intermediate rear axle shaft failure. Adv Automob Eng. 2015; 4:1–3. https://doi.org/10.4172/2167 – 7670.1000114
12. Pantazopoulos GA. A short review on fracture mechanisms of mechanical components operated under industrial conditions: Fractographic analysis and selected prevention strategies. Metals. 2019; 9(2):148. https://doi.org/10.3390/met9020148
13. Papadopoulou S, Vazdirvanidis A, Toulfatzis A, Rikos A, Pantazopoulos G. Failure investigation of products and components in metal forming industry: Root cause analysis and process – based approach. J Fail Anal Prev. 2020; 20(1):106–114. https://doi.org/10.1007/s11668 – 020 – 00801 – 4
14. Kurhade A, Talele V, Rao TV, Chandak A, Mathew VK. Computational study of PCM cooling for the electronic circuit of smartphones. Materials Today: Proceedings. 2021; 47:3171–3176. https://doi.org/10.1016/j.matpr.2021.06.284
15. Kurhade AS, Siraskar GD, Deshmukh MT, Patil PA, Chaudhari SS, Kadam AA, Dolas AS, Mahajan RG, Waware SY, Yadav RS. Impact of PCM on heat dissipation from IC chips. J Mines Met Fuels. 2025; 73(3):717–724. https://doi.org/10.18311/jmmf/2025/47522
16. Kurhade AS, Murali G. Thermal control of IC chips using phase change material: A CFD investigation. Int J Mod Phys C. 2022; 33(12):2250159. https://doi.org/10.1142/S0129183122501595
17. Kurhade AS, Murali G, Rao TV. CFD Approach for Thermal Management to Enhance the Reliability of IC Chips.
18. Waware SY, Kore SS, Kurhade AS, Patil SP. Innovative heat transfer enhancement in tubular heat exchanger: An experimental investigation with minijet impingement. J Adv Res Fluid Mech Therm Sc. 2024; 116(2):51–58. https://doi.org/10.37934/arfmts.116.2.5158
19. Kurhade AS, Biradar R, Yadav RS, Patil P, Kardekar NB, Waware SY, Munde KH, Nimbalkar AG, Murali G. Predictive placement of IC chips using ANN – GA approach for efficient thermal cooling. J Adv Res Fluid Mech Therm Sc. 2024; 118(2):137–144. https://doi.org/10.37934/arfmts.121.1.137147

20. Waware SY, Chougule SM, Yadav RS, Biradar R, Patil P, Munde KH, Kardekar NB, Nimbalkar AG, Kurhade AS, Murali G, Kore SS. A comprehensive evaluation of recent studies investigating nanofluids utilization in heat exchangers. J Adv Res Fluid Mech Therm Sci. 2024; 119(2):160–172. https://doi.org/10.37934/arfmts.119.2.160172
21. Upadhe SN, Mhamane SC, Kurhade AS, Bapat PV, Dhavale DB, Kore LJ. Water – saving and hygienic faucets for public places in developing countries. InTechno – Societal 2018: Proceedings of the 2nd International Conference on Advanced Technologies for Societal Applications – Volume 1 2020; pp. 617–624. Springer International Publishing. https://doi.org/10.1007/978 – 3 – 030 – 16848 – 3_56
22. Sidhappa KA, Hande MS, Patil MS, Mask MV. Heat transfer enhancement by using twisted tape inserts with circular holes in forced convection. Int Jo Innov Eng Res Technol. 2016; 3(3):1–7.
23. Kurhade AS, Kardekar NB, Bhambare PS, Waware SY, Yadav RS, Pawar P, Kirpekar S. A comprehensive review of electronic cooling technologies in harsh field environments: obstacles, progress, and prospects. J Mines Met Fuels. 2024; 72 (6): 557–579. https://doi.org/10.18311/jmmf/2024/45212
24. Kurhade AS, Waware SY, Bhambare PS, Biradar R, Yadav RS, Patil VN. A comprehensive study on *Calophyllum inophyllum* biodiesel and dimethyl carbonate blends: Performance optimization and emission control in diesel engines. J Mines Met Fuels. 2024; 72 (5):499–507. https://doi.org/10.18311/jmmf/2024/45188
25. Kurhade AS, Waware SY, Munde KH, Biradar R, Yadav RS, Patil P, Patil VN, Dalvi SA. Performance of solar collector using recycled aluminium cans for drying. J Mines Met Fuels. 2024; 72 (5):455–461. https://doi.org/10.18311/jmmf/2024/44643
26. Kurhade AS, Siraskar GD, Bhambare PS, Dixit SM, Waware SY. Numerical investigation on the influence of substrate board thermal conductivity on electronic component temperature regulation. J Adv Res Numer Heat Trans. 2024; 23(1):28–37. https://doi.org/10.37934/arnht.23.1.2837
27. Kurhade AS, Siraskar GD, Kondhalkar GE, Darade MM, Yadav RS, Biradar R, Waware SY, Charwad GA. Optimizing aerofoil design: A comprehensive analysis of aerodynamic efficiency through CFD simulations and wind tunnel experiments. J Mines Met Fuels. 2024: 713–724. https://doi.org/10.18311/jmmf/2024/45361
28. Kurhade AS, Siraskar GD, Darade MM, Dhumal JR, Kardile CS, Biradar R, Patil SP, Waware SY. Predicting heat transfer enhancement with twisted tape inserts using fuzzy logic techniques in heat exchangers. J Mines Met Fuels 2024; 743–750. https://doi.org/10.18311/jmmf/2024/45348
29. Kurhade AS, Kadam AA, Biradar R, Bhambare PS, Gadekar T, Patil P, Yadav RS, Waware SY. Experimental investigation of heat transfer from symmetric and asymmetric IC Chips mounted on the SMPS board with and without PCM. J Adv Res Fluid Mech Therm Sc. 2024; 121(1):137. https://doi.org/10.37934/arfmts.121.1.137147
30. Patil P, Kardekar N, Yadav R, Kurhade A, Kamble D. Nanofluids: An experimental study for MQL Grinding. J Mines Met Fuels. 2023; 71(12):2751–2756. https://doi.org/10.18311/jmmf/2023/41766
31. Kurhade AS, Bhambare PS, Desai VP, Murali G, Yadav RS, Patil P, Gadekar T, Biradar R, Kirpekar S, Charwad GA, Waware SY. Investigating the effect of heat transfer influenced by the application of wavy corrugated twisted tape inserts in double pipe heat exchangers. J Adv Res Fluid Mech Therm Sc.[Internet]. 2024; 122(2):146–155. https://doi.org/10.37934/arfmts.122.2.146155
32. Kurhade AS, Murali G, Jadhav PA, Bhambare PS, Waware SY, Gadekar T, Yadav RS, Biradar R, Patil P. Performance analysis of corrugated twisted tape inserts for heat transfer augmentation. J Adv Res Fluid Mech Therm Sci. 2024; 121(2):192–200. https://doi.org/10.37934/arfmts.121.2.192200
33. Kurhade MA, Dange MM, Nalawade DB. Effect of wavy (Corrugated) twisted tape inserts on heat transfer in a double pipe heat exchanger. Int J Innov Engineering Res Technol. 2015; 2(1):1–8.
34. Kurhade AS, Gadekar T, Siraskar GD, Jawalkar SS, Biradar R, Kadam AA, Yadav RS, Dalvi SA, Waware SY, Mali CN. Thermal performance analysis of electronic components on different substrate materials. J Mines Mets Fuels. 2024; 1093–8. https://doi.org/10.18311/jmmf/2024/45569
35. Kurhade AS, Siraskar GD, Chekuri RBR, Murali G, Pawar P, Patil AR, Waware SY, Yadav RS. Biodiesel blends: A sustainable solution for diesel engine performance improvement. J Mines Mets Fuels. 2025; 73(3):839-47. https://doi.org/10.18311/jmmf/2025/47628
36. Kurhade AS, Siraskar GD, Jawalkar SS, Gadekar T, Bhambare PS, Biradar R, Yadav RS, Waware SY, Mali CN. The impact of circular holes in twisted tape inserts on forced convection heat transfer. J Mines Met Fuels. 2024; 72(9):1005–1012 [Internet]. https://doi.org/10.18311/jmmf/2024/45505
37. Kurhade AS, Darade MM, Siraskar GD, Biradar R, Mahajan RG, Kardile CS, Waware SY, Yadav RS.

State – of – the – art cooling solutions for electronic devices operating in harsh conditions. J Mines Met Fuels. 2024; 843–861. https://doi.org/10.18311/jmmf/2024/45374

38. Kurhade AS, Warke P, Maniyar K, Bhambare PS, Waware SY, Deshpande S, Harsur S, Ingle M, Kolhe P, Patil PA, Jadhav P. The wind rose analysis of temperature variation with sensor implantation technique for a wind turbine. J Adv Res Fluid Mech Therm Sci. 2024; 122(1):1–8. https://doi.org/10.37934/arfmts.122.1.118
39. Kurhade AS, Siraskar GD, Bhambare PS, Keloth D, Kaithari SM, Waware SY. Enhancing smartphone circuit cooling: A Computational Study of PCM Integration. J Adv Res Numer Heat Trans. 2024; 27(1):132–145. https://doi.org/10.37934/arnht.27.1.132145
40. Yadav RS, Gadekar T, Gundage V, Patil P, Patil A, Patil P, Patil A, Sutar R, Kurhade AS. Numerical and experimental investigation of the effect of overlapping angle on strength and deformation of curved plate joined using arc welding process. J Mines Met Fuels. 2024: 1059–1066. https://doi.org/10.18311/jmmf/2024/45697
41. Yadav RS, Nimbalkar A, Gadekar T, Patil P, Patil VN, Gholap AB, Kurhade AS, Dhumal JR, Waware SY. Comparison of experimental and numerical investigation of mono – composite and metal leaf spring. J Mines Metals Fuels. 2024: 815–827. https://doi.org/10.18311/jmmf/2024/45325
42. Deshpande SV, Pawar RS, Keche AJ, Kurhade A. Real – time surface finish measurement of stepped holding shaft by automatic system. J Adv Manuf Syst. 2025. https://doi.org/10.1142/S0219686725500386
43. Kurhade AS, Siraskar GD, Bhambare PS, Murali G, Deshpande SV, Warke PS, Waware SY. Simulation and analysis of heat transfer in counter – flow helical double – pipe heat exchangers Using CFD. Int J Mod Phys C. 2025. https://doi.org/10.1142/S0129183125500433
44. Parkar A, Yadav RS, Chopade R, Dhavase N, Dhumal JR, Mankar SP, Patil S, Ghuge K, Giri B, Kurhade AS. Automating the two – dimensional design of heating, ventilation, air conditioning and refrigeration (HVACR) Ducts using Computer Programming Language: An Algorithmic Approach. J Mines Met Fuels. 2025; 211–220. https://doi.org/10.18311/jmmf/2025/47335
45. Kurhade AS, Siraskar GD, Darade MM, Murali G, Katkar TR, Patil SP, Charwad GA, Waware SY, Yadav RS. Enhancement in heat transfer with nanofluids in double – pipe heat exchangers. J Mines Met Fuels. 2025; 165–172. https://doi.org/10.18311/jmmf/2025/47225
46. Kurhade AS, Chougule SM, Kharat PV, Kondhalkar GE, Murali G, Raut PN, Charwad GA, Waware SY, Yadav RS. Integrated approach to enhance vehicle safety: A novel bumper design with energy – absorbing mechanisms. J Mines Met Fuels. 2025; 27–35. https://doi.org/10.18311/jmmf/2025/47168
47. Raut PN, Dolas AS, Chougule SM, Darade MM, Murali G, Waware SY, Kurhade AS. Green adsorbents for heavy metal removal: A study on zinc ion uptake by *Tinospora cordifolia* biocarbon. J Mines Met Fuels. 2025; 21–25. https://doi.org/10.18311/jmmf/2025/47121
48. Yadav R, Nimbalkar A, Kirpekar S, Patil PJ, Dalvi SA, Jadhav PA, Kurhade AS, Wakchaure GN. Effect of transformed – induced plasticity steel plate thickness on ultimate tensile strength of butt welded joint using Nd: YAG laser. Int J Veh Struct Syst. 2024; 16(6).
49. Yadav RS, Gandhi P, Veeranjaneyulu K, Gaji R, Kirpekar S, Pawar D, Khairnar YS, Patil S, Kurhade AS, Patil SP. Influence of plate thickness on the mechanical behaviour of mild steel curved plates: An experimental study. J Mines Met Fuels. 2024; 1319–1327. https://doi.org/10.18311/jmmf/2024/46253
50. Kurhade AS, Bhambare PS, Siraskar GD, Mukesh S, Dixit PS, Waware SY. Computational study on thermal management of IC chips with phase change materials.
51. Kurhade MA, Dange MM, Nalawade DB. Fuzzy logic modelling of heat transfer in a double pipe heat exchanger with wavy (corrugated) twisted tape inserts. Int J Innov Eng Res Technol. 2(1):1–8.